ELSEVIER

Biophysical Chemistry 117 (2005) 47 – 53

Biophysical Chemistry

http://www.elsevier.com/locate/biophyschem

Morphology and gelation of thermosensitive chitosan hydrogels

K.E. Crompton[a,b], R.J. Prankerd[c], D.M. Paganin[a], T.F. Scott[a], M.K. Horne[d], D.I. Finkelstein[d], K.A. Gross[a], J.S. Forsythe[a,b,*]

[a]*School of Physics and Materials Engineering, Monash University, Wellington Rd, Clayton, VIC 3800, Australia*
[b]*CRC for Polymers, 32 Business Park Drive, Notting Hill, VIC 3168, Australia*
[c]*Department of Pharmaceutics, Victorian College of Pharmacy, Monash University, 381 Royal Parade, Parkville, VIC 3052, Australia*
[d]*Howard Florey Institute, Gate 11, Royal Parade, The University of Melbourne, VIC 3010, Australia*

Received 21 February 2005; accepted 11 March 2005
Available online 17 May 2005

Abstract

The morphology of physical hydrogels is often difficult to examine due to the delicate nature of the system and therefore has not been studied in detail. Chitosan/GP (glycerophosphate salt) is a significant hydrogel in the biomedical and cosmetic fields as it is thermosensitive and contains less than 5% polysaccharide. The morphology of this system was examined with laser scanning confocal microscopy (LSCM) to image the gel morphology. The images indicate that the gel is quite heterogeneous, and power spectra reveal a fractal-like morphology. A study of composition found that increasing chitosan concentration increased the amount of polymer-rich phase present in the gel, and that the smallest aggregates decreased in size.

Keywords: Chitosan; Thermally responsive material; Confocal microscopy; Polysaccharide

1. Introduction

Hydrogels are an ideal class of polymeric material for biomedical applications. They contain only small amounts of polymeric material (typically hydrogels are in the range 1–30 wt.% in aqueous solvent), have low interfacial tension, high molecular and oxygen permeability and mechanical properties that resemble physiological soft tissue [1]. Hydrogels are used for cell encapsulation [2–5], lubrication and cushioning of joints [6,7], drug delivery [8–13] or tissue-engineered scaffolds [13–16]. Drug release profiles, the flow of nutrients to seeded cells and enzymatic degradation are all diffusion-controlled, which is determined by interconnected porosity and volume of water phase present. The shape, size, and size distribution of pores are also important parameters for the seeding of cells within the hydrogel. To fully exploit a hydrogel, these morphological characteristics must be known and controlled or tailored for the intended application.

Many techniques are available for microstructural analysis of macro-porous hydrogels, however most raise issues such as collapse of pore structure during dehydration [16–18] and lack of contrast and resolution. Laser scanning confocal microscopy (LSCM) bypasses these issues by imaging hydrogel morphology in the native hydrated state and has a resolution of 0.35 μm (for a more comprehensive description see Srinivasarao [19]). Conjugation of a water-soluble fluorochrome to the material to provide contrast is important. The conjugated fluorophore is assumed to have minimal effect on the behaviour of the hydrogel [20], because the hydrogel molecules are thousands of times larger and more concentrated than the fluorophore (e.g., in this instance, the molar ratio of chitosan amine to fluorescein isothiocyanate (FITC) is 66,000:1).

Chitosan is a polysaccharide hydrogel. It is composed of (1,4)-linked 2-amino-2-deoxy-β-D-glucan (Fig. 1),

* Corresponding author. School of Physics and Materials Engineering, Monash University, Wellington Rd, Clayton, VIC 3800, Australia. Tel.: +61 3 9905 9609; fax: +61 3 9905 4940.
E-mail address: John.Forsythe@spme.monash.edu.au (J.S. Forsythe).

0301-4622/$ - see front matter © 2005 Elsevier B.V. All rights reserved.
doi:10.1016/j.bpc.2005.03.009

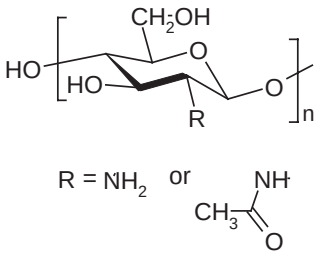

Fig. 1. Chemical structure of chitosan.

produced by deacetylating chitin, with applications ranging from biomedical to cosmetic. The properties of chitosan are primarily governed by the degree of deacetylation (DD, determined from the relative amounts of acetyl and amine groups at the C2 position, labelled R in Fig. 1).

Chitosan is soluble in dilute acidic solutions, but phase-separates at pH > 6 to form a hydrogel. However, on addition of glycerophosphate salt (GP) to a chitosan solution, the pH can be raised to neutral without causing phase-separation [21,22]. The system becomes thermally sensitive, forming a gel above a certain temperature. To date, the only study of chitosan/GP morphology known to the authors was conducted after freeze-drying, by SEM [9]. This study aims to examine the morphology of chitosan/GP, in its native, hydrated state, and to gain a better understanding of the gelation mechanism.

2. Methodology

2.1. Materials

Chitosan (Sigma) was purified by dissolving in 0.1 M HCl (BDH), filtering through grade 3 filter paper (Whatman), heating, and then when cooled, stirring with granulated carbon and refiltering. The chitosan was precipitated by adding 100 mL chitosan solution drop wise to 600 mL 0.1 M KOH (Aldrich). The precipitate was collected, rinsed twice with distilled deionised water, and freeze-dried for 48 h. β-Glycerophosphate disodium salt (Sigma) was used as received, while the fluorophore FITC (Aldrich) was dissolved to 100 μM before using for LSCM.

2.2. Sample preparation

Sample solutions were made by dissolving chitosan in dilute aqueous HCl to a molar ratio of 0.9:1 with chitosan amine group, to a range of concentrations (given in Table 1). While in an ice bath, 2.6 M GP was added drop wise to the solutions, to a molar ratio of 12:1 with chitosan. The pH of the solutions was monitored throughout GP addition. For confocal microscopy, an addition of FITC to a final concentration of 9 μM was used.

2.3. ^{13}C Cross polarisation magic angle spinning nuclear magnetic resonance (CP/MAS NMR) spectroscopy

In order to determine the degree of deacetylation, high-resolution solid state ^{13}C CP/MAS NMR was undertaken on a Varian Unity Plus spectrometer at room temperature using a chitosan sample previously dried in a vacuum oven at room temperature. The resonance frequency used was 75 MHz, contact time 1 ms (optimised by measuring in the range of 10 μs to 10 ms), while the relaxation delay time was 2 or 5 s. The 90° pulse was of 4.5 μs and the spinning rate for MAS was 8–10 kHz. The degree of deacetylation was 85 ± 2% and was determined by integrating the CH_3 absorbance (24 ppm) and the C-1 absorbance (105 ppm).

2.4. Scanning electron microscopy

Samples were prepared as for LSCM, but once gelled on the microscope slide the samples were frozen in liquid nitrogen and lyophilised for 24 h. These were then sputter-coated with gold (Bal-Tec SCD 005, Balzers) for 3 min and imaged on a Hitachi S-570 SEM using an accelerating voltage of 10 kV.

2.5. Laser scanning confocal microscopy

0.1 mL of sample solution was pipetted onto a microscope slide with a 0.5 mm spacer, before a number 1.5 glass cover slip (Lomb Scientific) was placed on top, sealing the space and preventing syneresis (water loss was < 0.5%). The sample was then heated at 37 °C for 2 min (a ramp rate of approximately 10 °C/min). A Fluoview 1000 LSCM, with an Olympus 60× water lens (numerical aperture 1.00) was used. Three images from random locations within each sample were taken, and two samples were used for each composition.

A median filter was applied to each image to remove isolated erroneous pixels without modifying edges, and the contrast was then optimised by ignoring 3% of the brightest and darkest pixels and spreading the intensity range of the remaining pixels linearly to cover the maximum available value range.

Table 1
Sample compositions, prepared with the addition of GP to a molar ratio of 12:1 with chitosan

Chitosan concentration (wt.%/vol.%)	0.15	0.25	0.3	0.5	0.75	0.85	1.0	1.25
Acid concentration (M)	0.009	0.013	0.017	0.028	0.043	0.055	0.061	0.079

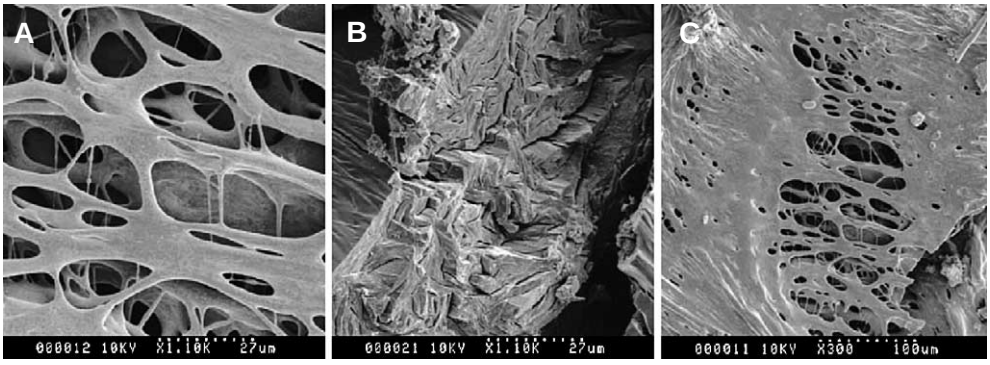

Fig. 2. SEM images of lyophilised chitosan/GP. A) 0.5 wt.%/vol.%, showing the porous structure; B) fracture surface of 1.0 wt.%/vol.%, showing the majority crushed structure; C) 0.5 wt.%/vol.% showing a skin layer around the revealed inner pores.

2.6. Light scattering

Cloud point measurements (turbidity) were taken at a wavelength of 500 nm, isothermally at 37 °C in a purpose-made sample holder with metal sides and base, volume 2 mL, to promote thermal conduction. Each sample was measured in triplicate.

2.7. Rheology

Rheological measurements of phase shift (tan $\delta = G''/G'$), were taken on a Bohlin CS-50 rheometer in parallel plate configuration, after ensuring that the linear viscoelastic regime was used. Isothermal studies were conducted at 37 °C, angular frequency of 0.3, and under 3 Hz, to reveal the induction time of gelation (taken to be the time at which tan δ is frequency independent).

3. Results and discussion

3.1. Scanning electron microscopy

The morphology of the dry chitosan/GP gels was initially examined by SEM. Fig. 2 shows sample SEM images of two concentrations, of which Fig. 2A is typical. It shows a very fibrous microstructure, with large interconnected areas between fibres.

Fig. 2B, taken at a fracture surface to reveal the bulk microstructure, shows that during water loss much of the pore structure is compacted. At the surface, however, a different effect is seen. While the fibrous structure exists, a skin layer has formed (Fig. 2C). This confirms reports in the literature that hydrogels form skin layers due to dehydration at the surface during gelation [23–25].

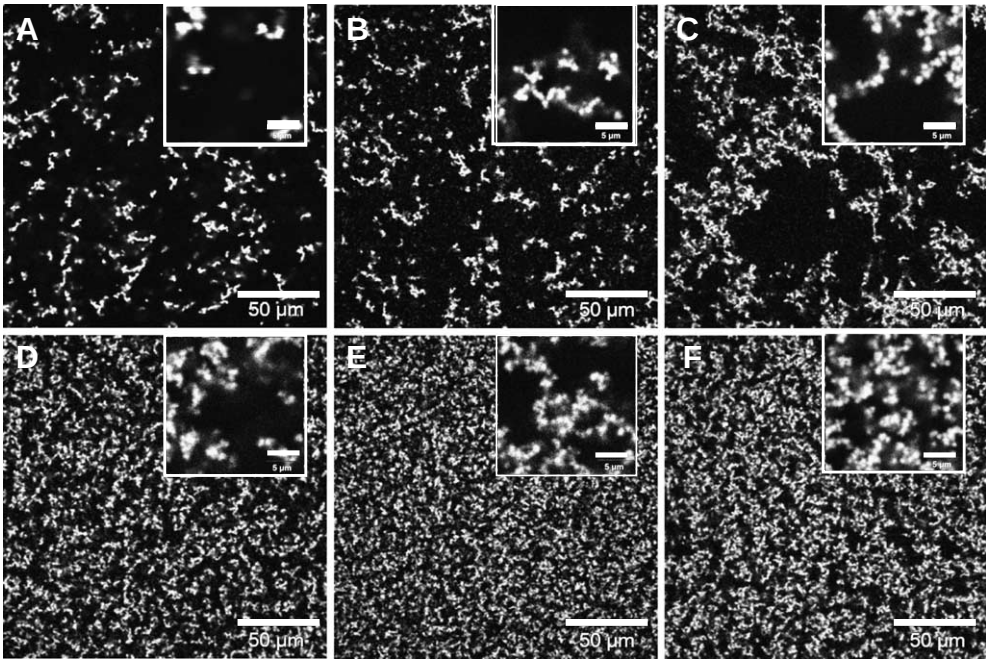

Fig. 3. Microstructural images from LSCM, inset optically magnified 10X. Chitosan compositions: A) 0.25 wt.%/vol.%, B) 0. 5 wt.%/vol.%, C) 0.75 wt.%/vol.%, D) 1.0 wt.%/vol.%, E) 1.25 wt.%/vol.%, F) 1.5 wt.%/vol.%. White areas represent the polymer-rich phase; scale bars represent 50 μm, and 5 μm in inset.

3.2. Laser scanning confocal microscopy

Chitosan/GP of a range of concentrations was examined by LSCM. Chitosan/GP was found to have a beaded, open structure (Figs. 3 and 4), forming a network by linking polymeric aggregates in agglomerates and chains. The overall appearance of the gel structure observed with LSCM was quite different to the images provided by SEM. SEM failed to detect the fine aggregate structure, although images such as in Fig. 2 are at higher magnification than those in Fig. 3. Upon dehydration, the polymeric aggregates seen with LSCM have collapsed into the network structure, leaving a microstructure that is very different to the hydrogel.

Most physical gels are formed by spinodal decomposition, a non-equilibrium phase-separation mechanism [26–29]. During spinodal decomposition, temperature change causes the single-phase solution to become unstable and concentration fluctuations to form, which over time become distinct phases as the difference in composition in neighbouring areas increases. Recently, it was found that nucleation and growth is an alternative mechanism for phase separation of physical gels [26,30], although it is more common for crystalline materials. Nucleation and growth occurs when the temperature change causes the single-phase solution to move into a metastable, rather than unstable, region. At this point, a second phase develops which over time grows in size but does not change in composition. During nucleation, the polymeric phase is composed of many small regions, which during the growth phase will expand (Ostwald ripening) and possibly connect. The microstructure of a material can be indicative of the phase-separation mechanism, and the microstructure that develops from spinodal decomposition is well known from simulation studies [31,32]. The morphology of the chitosan/GP gels is quite different from typical spinodal decomposition microstructure. It more closely resembles a structure expected during nucleation and growth [33], although further studies are necessary to make a definitive assignment.

The confocal images in Fig. 3 show that the polymer-rich phase increased with increasing chitosan composition.

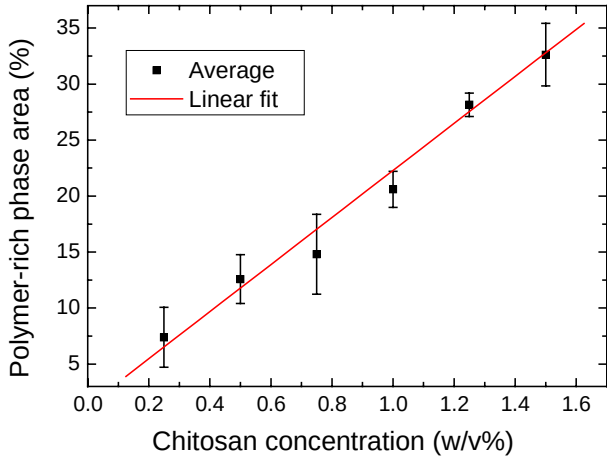

Fig. 5. Phase analysis of LSCM images (number of samples=6 for each composition).

Phase analysis revealed a linear trend in the amount of polymer-rich phase in each field of view (Fig. 5). The composition of chitosan ranges from 0.25 to 1.5 wt.%/vol.%, however the phase analysis shows that the amount of polymer-rich phase ranges from 7% to 33%. Therefore, the chitosan is still highly hydrated within this phase, and the polymer chains are loosely packed.

The LSCM images show that the size of the aggregate was of the order of 1–5 μm, and decreased with increasing chitosan concentration. The size of the aggregates was incorporated into a distribution of all length scales (frequencies) present. A power spectrum is an example of this distribution, which can be determined by taking the 2D Fourier transform (FT) of each image. A similar technique was used to analyse distances in pNIPAAm, and fibrin gels [34,35]. The FT was taken of unfiltered and unoptimised images. The power spectrum is a function of wavenumber, q, where $q=2\pi/d$, d is the associated length scale, in this case equal to NL/i. Here, i is the distance in pixels from the central pixel in the Fourier-transformed array, N is the size of the array in pixels (512), and L is the length of each pixel (0.414 μm, or 0.0414 μm for the 10× optically magnified images). The 2D FT has $q=0$ at its centre, i.e. when $i=N/2$. If the

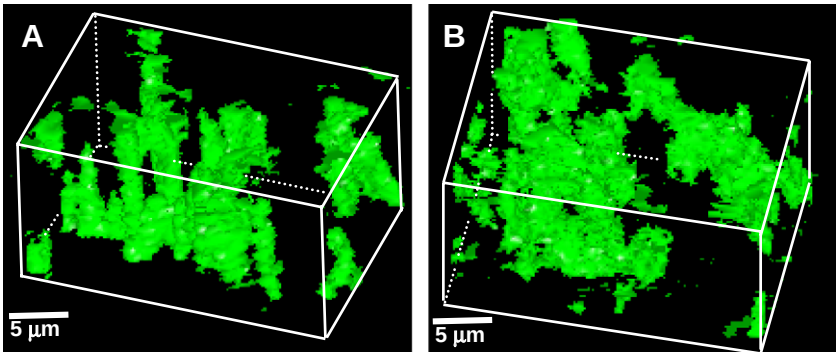

Fig. 4. Three-dimensional visualisations of chitosan/GP gels, using stacked LSCM images. A) 0.25 wt.%/vol.% chitosan, B) 1.0 wt.%/vol.% chitosan.

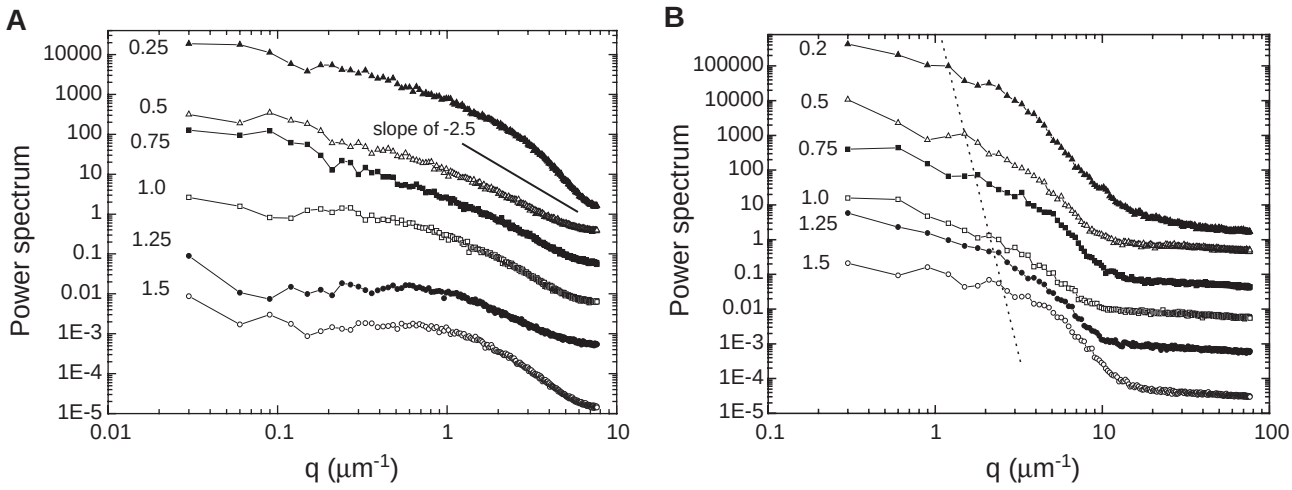

Fig. 6. Power spectra of LSCM images of a range of chitosan concentrations (in wt.%/vol.%), A) 60× images, B) 600× images. The dotted line calls attention to shifting peaks. The curves have been vertically shifted for easy comparison.

microstructure was randomly oriented in each dimension throughout the bulk, the squared modulus of the 2D FT could be circularly averaged — for this reason images were taken at 0.4 μm intervals to a depth of 10 μm and visualised in 3D (see Fig. 4) to ensure completely random microstructure in all dimensions. The power spectrum is related to the structure factor of the material, $S(q)$, which is the Fourier transform of length scales (frequencies) between areas of different density within the sample (the density correlation function), and is important in network structures. Sample power spectra for each composition can be found in Fig. 6.

The two most important features of a power spectrum are the presence of any peaks, indicating that the length scale in question occurs often; and the slope of the curve at high q, which describes the boundary between phases. The power spectra of chitosan/GP LSCM images do not have any well-defined peaks to describe distance between aggregates, which would be found at the 60× magnification. Many small, ill-defined peaks are found in the power spectra, indicating that there are many common length-scales within the sample, rather than either a mono-disperse or wide distribution. The gels are therefore quite heterogeneous. The power spectra from the 600× magnification images also show a heterogeneous structure, expected on this length scale as the aggregates have agglomerated into randomly-sized regions, but at the q-values that corresponds to the aggregate diameter there are distinct, although small peaks, which move to higher q with increasing chitosan composition. The peak is therefore a good measure of change in aggregate size with composition — an increase in q corresponds to an overall decrease in aggregate size (Fig. 7).

The slopes of the power spectra are uniform, at -2.5 ± 0.8, which indicates a weakly segregated, fractal-like structure [36]. This is not uncommon in hydrogel formation [26,34,37–39]. Small and ultra-small angle neutron studies (SANS and USANS) are currently underway to evaluate the fractal dimension of the gel.

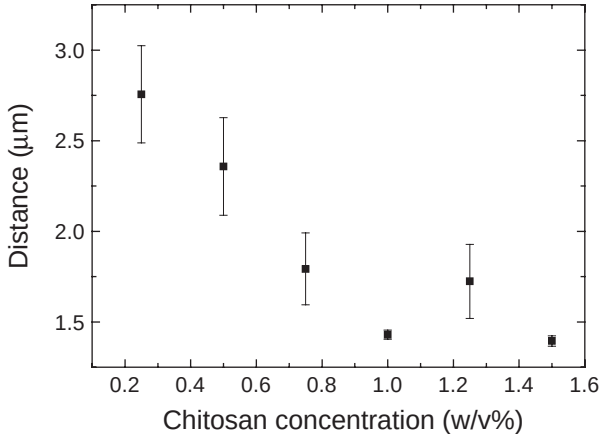

Fig. 7. The lengths calculated from peaks in the power spectra of 600× LSCM images as a function of chitosan composition correspond to aggregate diameter and larger agglomerates.

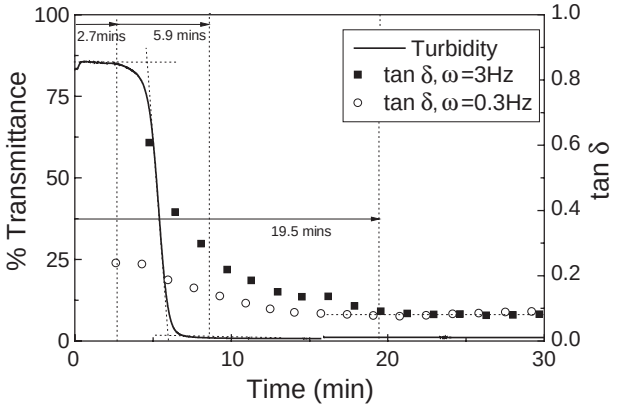

Fig. 8. Gelation of 1.25 wt.%/vol.% chitosan/GP as measured by light scattering and rheology. The period of induction of gelation is clearly shown, also the length of time for gelation to go to completion.

3.3. Light scattering and rheology

The time until phase separation and complete gelation were examined by two different techniques, light scattering and rheology respectively (Fig. 8). The turbidity measurements taken by light scattering showed that phase separation for all samples ranged from 4 to 9 min, whereas rheological measurements of tan δ revealed a much longer time to gelation of 18–25 min (the time at which the tan δ becomes frequency independent). The difference in these values reflects the measurement taking place — the time to phase separation taken from light scattering measures the time until the phase-regions are large enough to deflect or block light through the sample. Rheology measures the mechanical properties of the forming gel, related to the bulk macrostructure. In this case, the time to gelation takes into account aggregation on all length scales, when the gel is solid rather than liquid-like. Thus, physical cross-links form some time after phase separation has begun.

4. Conclusion

Chitosan/GP is a low composition thermosensitive hydrogel, and hence examination of its morphology is difficult. This study shows that LSCM is a valuable technique for imaging hydrogel microstructure, giving both qualitative and quantitative data. The microstructure of dehydrated chitosan/GP is very different from the gel, and composition was found to play a role in determining the microstructure. The images of chitosan/GP by LSCM show a heterogeneous microstructure and suggest that the kinetic gelation mechanism of this system may be nucleation and growth.

Acknowledgements

We would like to thank W. Cook for use of the UV–vis spectrophotometer, and I. Harper, M. Kitchen, and J. Gillam for useful discussions on LSCM data analysis. This project was funded by an Australian Postgraduate Award, the CRC for Polymers and ARC project DP0450618.

References

[1] B.D. Ratner, A.S. Hoffman, Synthetic hydrogels for biomedical applications, in: J.D. Andrade (Ed.), Hydrogels for Medical and Related Applications, ACS, Washington, DC, 1976, pp. 1–36.
[2] B.A. Zielinski, P. Aebischer, Chitosan as a matrix for mammalian cell encapsulation, Biomaterials 15 (13) (1994) 1049–1056.
[3] D.F. Emerich, S.R. Winn, L. Christenson, M.A. Palmatier, F.T. Gentile, P.R. Sanberg, A novel approach to neural transplantation in Parkinson's disease: use of polymer-encapsulated cell therapy, Neurosci. Biobehav. Rev. 16 (1992) 437–447.
[4] P. Aebischer, P.A. Tresco, S.R. Winn, L.A. Greene, C.B. Jaeger, Long-term cross-species brain transplantation of a polymer-encapsulated dopamine-secreting cell line, Exp. Neurol. 111 (1991) 269–275.
[5] P. Aebischer, L. Wahlberg, P.A. Tresco, S.R. Winn, Macroencapsulation of dopamine-secreting cells by coextrusion with an organic polymer solution, Biomaterials 12 (1991) 50–56.
[6] R. Barbucci, S. Lamponi, A. Borzacchiello, L. Ambrosio, M. Fini, P. Torricelli, R. Giardino, Hyaluronic acid hydrogel in the treatment of osteoarthritis, Biomaterials 23 (23) (2002) 4503–4513.
[7] C.D. Hoemann, J.D. Sun, A. Legare, M.D. McKee, P. Ranger, M.D. Buschmann, A thermosensitive polysaccharide gel for cell delivery in cartilage repair, Trans. Ortho. Res. Soc. 26 (2001) 626.
[8] S. Miyazaki, F. Suisha, N. Kawasaki, M. Shirakawa, K. Yamatoya, D. Attwood, Thermally reversible xyloglucan gels as vehicles for rectal drug delivery, J. Control. Release 56 (1998) 75–83.
[9] E. Ruel-Gariépy, A. Chenite, C. Chaput, S. Guirguis, J.-C. Leroux, Characterization of thermosensitive chitosan gels for the sustained delivery of drugs, Int. J. Pharm. 203 (2000) 89–98.
[10] A.K. Andrianov, L.G. Payne, Polymeric carriers for oral uptake of microparticulates, Adv. Drug Deliv. Rev. 37 (1998) 155–170.
[11] J.L. Drury, D.L. Mooney, Hydrogels for tissue engineering: scaffold design variables and applications, Biomaterials 24 (24) (2003) 4337–4351.
[12] D. Cohn, A. Sosnik, A. Levy, Improved reverse thermo-responsive polymeric systems, Biomaterials 24 (2003) 3707–3714.
[13] H.L. Lai, A. Abu'Khalil, D.Q.M. Craig, The preparation and characterisation of drug-loaded alginate and chitosan sponges, Int. J. Pharm. 251 (2003) 175–181.
[14] T. Matsuda, T. Magoshi, Preparation of vinylated polysaccharides and photofabrication of tubular scaffolds as potential use in tissue engineering, Biomacromolecules 3 (2002) 942–950.
[15] S. Woerly, R. Marchand, C. Lavallee, Interactions of copolymeric poly(glyceryl methacrylate)-collagen hydrogels with neural tissue: effects of structure and polar groups, Biomaterials 12 (2) (1991) 197–203.
[16] R. Bellamkonda, J.P. Ranieri, N. Bouche, P. Aebischer, Hydrogel-based three-dimensional matrix for neural cells, J. Biomed. Mater. Res. 29 (5) (1995) 663–671.
[17] H. Trieu, S. Qutubuddin, Poly(vinyl alcohol) hydrogels: 2. Effects of processing parameters on structure and properties, Polymer 36 (13) (1995) 2531–2539.
[18] G.P. Dillon, Z. Yu, A. Sridharan, J.P. Ranieri, R.V. Bellamkonda, The influence of physical structure and charge on neurite extension in a 3D hydrogel scaffold, J. Biomater. Sci., Polym. Ed. 9 (10) (1998) 1049–1069.
[19] M. Srinivasarao, J.O. Park, Optical methods for three-dimensional visualization: photon tunneling microscopy and laser scanning confocal microscopy, in: R.F.J. Brady (Ed.), Comprehensive Desk Reference of Polymer Characterization and Analysis, American Chemical Society, Washington, DC, 2003, pp. 408–434.
[20] A. Lamprecht, U. Schäfer, C.-M. Lehr, Structural analysis of microparticles using confocal laser scanning microscopy, AAPS PharmSciTech 1 (3) (2000) (article 17).
[21] A. Chenite, C. Chaput, D. Wang, C. Combes, M.D. Buschmann, C.D. Hoemann, J.C. Leroux, B.L. Atkinson, F. Binette, A. Selmani, Novel injectable neutral solutions of chitosan form biodegradable gels in situ, Biomaterials 21 (2000) 2155–2161.
[22] A. Chenite, M. Buschmann, D. Wang, C. Chaput, N. Kandani, Rheological characterisation of thermogelling chitosan/glycerol-phosphate solutions, Carbohydr. Polym. 46 (2001) 39–46.
[23] Y.H. Bae, T. Okano, R. Hsu, S.W. Kim, Thermo-sensitive polymers as on–off switches for drug release, Makromol. Chem., Rapid Commun. 8 (1987) 481–485.
[24] S. Nayak, S.B. Debord, L.A. Lyon, Investigations into the deswelling dynamics and thermodynamics of thermoresponsive microgel composite films, Langmuir 19 (2003) 7374–7379.
[25] X. Zhang, R. Zhuo, Y. Yang, Using mixed solvent to synthesize temperature sensitive poly(*N*-isopropylacrylamide) gel with rapid dynamics properties, Biomaterials 23 (5) (2002) 1313–1318.

[26] C.-M. Chou, P.-D. Hong, Nucleation, growth, fractal aggregation, and late-stage coarsening on structural development of polymer physical gels, Macromolecules 37 (15) (2004) 5596–5606.
[27] F. Fergg, F.J. Keil, H. Quader, Investigations of the microscopic structure of poly(vinyl alcohol) hydrogels by confocal laser scanning microscopy, Colloid Polym. Sci. 279 (2001) 61–67.
[28] J.H. Aubert, Structural coarsening of demixed polymer solutions, Macromolecules 23 (1990) 1446–1452.
[29] S.W. Song, J.M. Torkelson, Coarsening effects on microstructure formation in isopycnic polymer solutions and membranes produced via thermally induced phase separation, Macromolecules 27 (1994) 6389–6397.
[30] C.-M. Chou, P.-D. Hong, A novel aspect on structural formation of physical gels, Macromolecules 36 (2003) 7331–7337.
[31] T. Taniguchi, A. Onuki, Network domain structure in viscoelastic phase separation, Phys. Rev. Lett. 77 (24) (1996) 4910–4913.
[32] A. Onuki, S. Puri, Spinodal decomposition in gels, Phys. Rev., E 59 (2) (1999) 1331–1334.
[33] T. Tanigami, H. Suzuki, K. Yamaura, S. Matsuzawa, Gelation and crystallization of poly(4-methyl-1-pentene) in cyclohexane solution, Macromolecules 18 (1985) 2595–2600.
[34] Y. Hirokawa, J. Jinnai, Y. Nishikawa, T. Okamoto, T. Hashimoto, Direct observation of internal structures in poly(*N*-isopropylacrylamide) chemical gels, Macromolecules 32 (1999) 7093–7099.
[35] A. Takahashi, R. Kita, T. Shinozaki, K. Kubota, M. Kaibara, Real space observation of three-dimensional network structure of hydrated fibrin gel, Colloid Polym. Sci. 281 (2003) 832–838.
[36] S.M. King, Small-angle neutron scattering, in: R.A. Pethrick, J.V. Dawkins (Eds.), Modern Techniques for Polymer Characterisation, John Wiley & Sons, New York, 1999, pp. 171–232.
[37] M. Manno, M.U. Palma, Fractal morphogenesis and interacting processes in gelation, Phys. Rev. Lett. 79 (21) (1997) 4286–4289.
[38] G. Pitarresi, G. Cavallaro, B. Carlisi, G. Giammona, D. Bulone, P.L. San Biagio, Novel hydrogels based on polyasparthydrazide. Synthesis and characterization, Macromol. Chem. Phys. 201 (17) (2000) 2542–2549.
[39] D. Renard, M.A.V. Axelos, F. Boue, J. Lefebvre, Small angle neutron scattering and viscoelasticity study of the colloidal structure of aqueous solutions and gels of a globular protein, J. Chim. Phys. Phys.-Chim. Biol. 93 (1996) 998–1015.